Seismic behavior of a caisson type breakwater on non-homogeneous soil deposits composed of liquefiable layer under earthquake loading

***X.H. Bao[1,2], †Dong Su[1], Y.B. Fu[1], and F. Zhang[3]**

[1]Department of Civil Engineering, Shenzhen University, China.
[2] Key Laboratory of Geotechnical and Underground Engineering, Ministry of Education, Tongji University, China
[3] Department of Civil Engineering, Nagoya Institute of Technology, Japan

*Presenting author: bxh@szu.edu.cn
†Corresponding author: sudong@szu.edu.cn

Abstract

Damage of breakwaters during earthquakes is mainly attributed to the liquefaction of foundation soil. Most of the studies have investigated the dynamic response of breakwaters considering uniform sand foundation and a single earthquake event. However, the foundation of a breakwater usually consists of many sub-layers of soil from liquefiable sand to relatively impermeable clay. Moreover, during earthquakes a main shock may trigger numerous aftershocks within a short time which may have the potential to cause additional damage to soil and structures. In this study, the performance of an existing caisson type breakwater on the natural ground composed of discontinuous liquefiable sand layer and impermeable clay layer is investigated using an effective based soil-water coupling finite element method. In the calculation, a real recorded seismic wave in the 2011 Great East Japan earthquake which composed of a main shock and two aftershocks is adopted as the input earthquake wave. The results reveal that time histories of excess pore water pressure is the governing factors to estimate the behavior of breakwater during and after an earthquake, and the repeated earthquake shakings have a significant effect on the accumulated displacement of breakwater and ground. Eventually the settlement is the most important aspect for the tsunami resistance capacity of breakwater structures.

Keywords: Caisson type breakwater, Repeated Earthquake shakings, Excess pore water pressure, Settlement, FEM.

Introduction

Earthquake induced liquefaction has become a major problem to offshore structures such as breakwaters, river dykes, levees, earth dams etc., supported on a cohesionless foundation soil. Previous studies have shown that the wide spread damage to offshore structures occurred mainly due to the liquefaction of foundation soil, resulting in settlement, tilting, slumping and lateral spreading (Seed 1968, Adalier et al. 1998, Huang & Yu 2013) [1]-[3]. Despite the extensive research and development of remedial measures to prevent the large deformation of soil structures, offshore structures have suffered severe damage during 2011 Great East Japan Earthquake (Oka et al. 2012, Mori et al. 2013, Mori et al. 2015) [4]-[6]. The minor to major damage was attributed due to the liquefaction of foundation soil. This event elucidates the further need to understand the deformation behavior of offshore structures resting on non-homogeneous liquefiable foundations. However, attention given to the seismic response of offshore structures under strong seismic loading is limited. Among these offshore structures, breakwaters may damage or lose their normal ability to resist tsunami loading during strong earthquake loading before the arriving of tsunami. To date, most of the investigations on breakwaters concentrated on the tsunami wave and the mechanical behavior of rubble mound (Fujima 2006, Imase et al. 2012, Susumu 2012, Takahashi et al. 2014) [7]-[10]. Experimental and numerical investigations on seismic behaviors of a composite breakwater under earthquake loading are still limited, which can be found in the works (Memos et al. 2003, Yuksel et al. 2004, Jafarian et al 2010, Ye 2012) [11]-[14].

On the other hand, most of the experimental studies and numerical analyses have been conducted previously to examine the behavior of offshore structures resting on uniform cohesionless soil during earthquakes (Aydingun & Adalier 2003, Adalier & Sharp 2004, Ye & Wang 2015) [15]-[17]. However, it is noted that natural soil deposits normally consist of many sub-layers with different soil particles and properties, ranging from sand to cohesive clay and coarse sand layers, referred to as non-homogeneous soil deposits. Huang et al. (2015) [18] point out that liquefaction in the saturated layer was the contributing factor to large settlement and sliding of the structures. Thus, the dynamic behavior of the breakwater on a liquefiable non-homogeneous foundation, consisting of discontinuous low permeability layers of silt or clay at different depths should be well understood.

During the earthquake that repeated ground-motion sequences occurring after short intervals of time, resulting from a main shock and aftershocks earthquakes (Zhang et al. 2013) [19], it was found that the low amplitude aftershock can accumulate large lateral deformation and continue for several minutes on the liquefied soil (Maharjan & Takahashi 2014) [20]. However, in most of the previous experimental and numerical studies seismic performance of soil structures is investigated by applying only a single earthquake, ignoring the influence of repeated shake phenomena. Among the limited studies considering the repeated earthquake shakings, Ye et al. (2007) [21] conducted shaking table tests and numerical analyses on saturated sandy soil to investigate the mechanical behavior of liquefiable foundations considering repeated shaking and consolidation processes. Xia et al. (2010) [22] presented numerical analysis of an earth embankment on liquefiable foundation soils under repeated shake and consolidation condition. During 2011 Great East Japan Earthquake, some structures continued to shake after the onset of soil liquefaction for more than two minutes. Moreover, during the reconnaissance survey after the earthquake, Sasaki et al. (2012) [23] found that the more severe deformation and subsidence of levees was due to the occurrence of aftershock, 30 min after the main shock. However, no previous study has examined the effects of repeated earthquake shakings on breakwaters lying on non-homogeneous soil deposits. Therefore, to understand the deformation mechanism of breakwaters resting on non-homogeneous soil deposits under main shock and sequential aftershocks is of great importance.

In this study, the co-seismic and post-seismic behavior of an existing caisson type breakwater resting on the natural ground composed of discontinuous clay and sand layer under the recorded seismic wave in the 2011 Great East Japan Earthquake which composed of a main shock and two aftershocks is investigated using an effective based soil-water coupling numerical model DBLEAVES (Ye 2011) [24]. In the analysis, an advanced elasto-plastic soil constitutive model named as Cyclic Mobility model (Zhang et al. 2007, Zhang et al. 2011) [25] [26] is used to describe the complicated nonlinear dynamic behavior of the foundation soils. The results show that the used numerical method is capable of capturing the progressive ground liquefaction and long-term consolidation process of the breakwater and foundation system during and after earthquake loading. The influence of earthquake can significantly reduce the capacity of breakwater to resist tsunami loading. In engineering practice, the settlement maybe a serious problem for the breakwater when its foundation ground composes of discontinuous impermeability clay and liquefiable sand soils.

Constitutive model

Using a proper constitutive model to accurately describe soil behaviors including the development of excess pore water pressure during earthquakes becomes a key factor when assessing the dynamic behavior of ground and foundation. In the studies using numerical methods, most of the previous investigations on seismic dynamics of offshore structures used simple constitutive models such as elastic or Mohr–Coulomb model to model the seabed soil (Ye & Wang 2015) [17]. These simple models are not capable of simulating the complicated nonlinear cyclic behaviors of soils and the failure process of offshore structures. Intensive nonlinear interaction between foundation and the structure cannot be effectively captured. Iai et al. (1998) [27] conducted effective stress analyses of port structures in Kobe port during the Hyogoken–Nambu earthquake in 1995. The numerical analyses calculated that the composite breakwater constructed on loose seabed soil settled about 2m during the event, which is consistent with the field observation. The work highlighted the importance of using effective stress analyses with well-calibrated cyclic soil model to realistically capture the nonlinear structure–foundation interaction. Therefore, it is very important to estimate the co-seismic and post-seismic behavior of breakwaters using an effective numerical method with proper constitutive model, for tsunami associated with the earthquake would cause serious damage to the structures especially when the foundation composed of liquefiable layer and might experience large deformation by earthquakes.

For this reason, by adopting the concepts of subloading (Hashiguchi & Ueno 1977) [28] and superloading (Asaoka et al. 2002) [29], Zhang et al. (2007) [25] proposed a rotational kinematic hardening elasto-plastic model named as Cyclic Mobility model (CM model) which can describe the mechanical behavior of soils under different drainage and loading conditions. Zhang et al. (20110 [26] and Ye B. et al. (2012) [30] extended the CM model to describe the mechanical behavior of soils under general three-dimensional stress conditions to consider the intermediate principal stress (Ye G.L. et al. 2012, Ye G.L. et al. 2013) [31] [32]. According to the work of shaking-table tests and numerical simulation under a repeated liquefaction-consolidation process by Ye B. et al. (2007) [33], it was confirmed that the static and dynamic behavior of sand could be well described by the CM model, considering the effect of the stress-induced anisotropy, the density and the structure of the soil formed in the natural sedimentary process, different loading conditions and drained conditions in a unified way.

In this study, the clay and sand are modeled with the above mentioned CM model. Eight parameters are employed in the model, among which five parameters, M, N, λ, κ and ν, are the same as those in the Cam-clay model. The other three parameters, a: the parameter controlling the collapse rate of the structure, m: the parameter controlling the loosing rate of the overconsolidation ratio or the change in density of the soil, and b_r: the parameter controlling the developing rate of the stress-induced anisotropy, have clear physical meanings and can be easily determined by undrained triaxial cyclic loading tests and drained triaxial compression tests. The values of eight parameters involved in the model are fixed in all loading process once they are determined from the laboratory tests. A detailed description of the CM model can be found in the references (Zhang et al. 2007, Zhang et al. 2011, Zhang et al. 2010) [25] [26] [34].

FEM model and parameters

Analysis range and soil profiles

The analysis range is shown in Fig.1, in which, the breakwater consisting of a caisson and rubble mound beneath, is constructed on a natural ground mainly composed of clay soil noted as Ac and sand soil noted as As. The original clay soil beneath rubble mound was replaced by sand noted as Rs. The caisson is made of concrete, and can be practically treated as an impermeable; while the rubble mound, which made of stones, is permeable. The total length of the analysis range is 240 m, and the distances from the centerline of breakwater to lateral sides of the ground foundation are both 120 m, which is considered to be large enough. The whole depth of the ground is 31 m, which composed of clay noted as Ac, sand noted as As and bottom sand noted as Ds. The depth of each soil layer and the size of breakwater are listed in Fig.1. Obviously, the liquefiable sand lay lied beneath thick clay layer which may prohibit the dissipation of pore water pressure. To improve the ground bearing capacity for structures, the original clay soil was replaced by sand beneath breakwater during project construction.

Some typical points on the breakwater and in the ground are chosen to illustrate the co-seismic and post-seismic behaviors of breakwater and foundation system. As shown in Fig. 1, the points on the breakwater are P-1 at the top of breakwater and P-2 at the bottom of caisson on rubble mound; the points beneath breakwater at the centerline are C-1 (GL-5 m) and C-2 (GL-15 m); the points in the near-filed of the ground (20 m away from the caisson) are N-0 (GL-0 m), N-1 (GL-5 m), N-2 (GL-15 m); the points in the far-filed of the ground (100 m away from the caisson) are F-0 (GL-0 m), F-1 (GL-5 m), F-2 (GL-15 m). Here, the locations with depth of 5 m and 15 m below ground surface in free field and beneath the breakwater are representative for the seismic behavior in upper clay layer and middle sand layer.

Ground parameters

As is known that the identification of parameters from laboratory and in situ tests is convincible, since no cyclic tests data of soils are available, some of these parameters were determined by element simulation with reference to the standard penetration tests. The average N-value and permeability for soils are listed in Table 1, while the eight ground parameters of each soil layer used in calculation are listed in Table 2. The initial values of the state variables employed in the constitutive model are listed in Table 3. On the other hand, the caisson which made of concrete is modeled as impermeable elastic solid element. The rubble mound, which made of stones, is modeled as permeable elastic solid element. The Physical properties of breakwater are listed in Table 4.

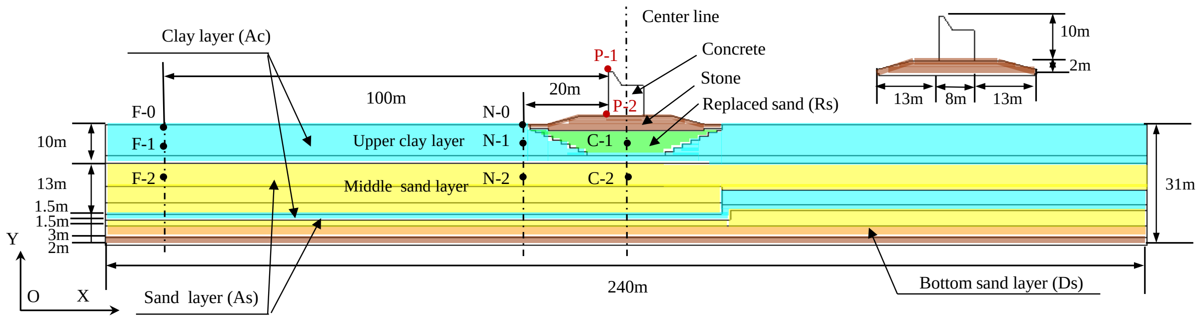

Figure 1. Soil profiles and section view of the caisson type breakwater

Analysis program and boundary condition

The numerical analysis was conducted using an effective stress based 2D/3D soil-water coupling program named as DBLEAVES (Ye 2011) [24], whose applicability and accuracy was firmly verified by the investigation on group-pile foundations in real scale (Jin et al. 2010) [35] and model tests (Bao et al. 2012, Bao et al. 2014) [36] [37]. Not only the instant reaction of ground and structure system when subjected to a strong earthquake but also the consequential long-term settlement of an alternately layered ground can be well examined using a sophisticated constitutive model and effective stress based soil-water coupling finite element method (Bao et al. 2016) [38].

For the boundary conditions, the base nodes of the ground foundation were assumed to be fixed in both x and y direction. The side boundary nodes at the same elevation were all “tied” together to experience the same accelerations. The earthquake loading is applied as a timevarying input acceleration to the foundation base. A constant water level is assumed and the drained boundary is set at the surface of the ground. As a large ocean wave is unlikely to occur simultaneously with earthquake, the wave loading is not considered in this study.

Table 1. The average N-value and permeability of ground soils

Layer	Clay Ac	Sand As	Replaced Rs	Ds
N-value	3	13	20	above 50
Permeability $\boldsymbol{k}$ (m/sec)	1×10^{-9}	1×10^{-4}	1×10^{-4}	4×10^{-5}

Table 2. Material parameters of ground soils

Layer	Ac	As	Rs	Ds
Compression index $\boldsymbol{\lambda}$	0.13	0.05	0. 05	0.046
Swelling index $\boldsymbol{\kappa}$	0.026	0.062	0.065	0.0061
Stress ratio of critical state **M**	1.21	1.41	1.42	1.42
Void ratio $\boldsymbol{N}$ (p'=98 kPa on *N.C.L.*)	1.08	0.93	0.92	0.88
Poisson's ratio $\boldsymbol{\nu}$	0.38	0.35	0.35	0.35
Degradation parameter of overconsolidation state $\boldsymbol{m}$	2.20	0.10	0.10	0.10
Degradation parameter of structure $\boldsymbol{a}$	0.10	2.20	2.20	2.20
Evolution parameter of anisotropy $\boldsymbol{b_r}$	0.10	1.50	1.50	1.50

Table 3. Initial values of the state variables of ground soils

Layer	Ac	As	Rs	Ds
Void ratio $\boldsymbol{e_0}$	0.97	0.98	0.91	0.81
Degree of structure $\boldsymbol{R_0^*}$	0.80	0.60	0.60	0.70
Overconsolidation ***OCR*** ($\boldsymbol{1/R_0}$)	2.00	3.00	4.00	20.0
Anisotropy $\boldsymbol{\zeta_0}$	0.0	0.0	0.0	0.0

Table 4. Physical properties of breakwater

Item	Elastic modulus (kPa)	Poisson's ratio $\boldsymbol{\nu}$	Density $\boldsymbol{\rho}$(t/m^3)	Permeability $\boldsymbol{k}$ (m/sec)
Caisson	1.0×10^{8}	0.25	2.5	1.0×10^{-11}
Rubble mound	1.0×10^{6}	0.30	2.0	1.0×10^{-2}

Earthquake loading and simulation stages

Input Earthquake wave

In the calculation, the seismic wave induced by the 2011 Great East Japan Earthquake (ML =9.0) is used as the earthquake loading to applied to the breakwater and foundation system. One of the main features of this earthquake is that the aftershock activity was extremely vigorous. The input earthquake motion recorded 2,300 m below ground surface at Urayasu in E-W direction is considered as being representative in Chiba Prefecture (source: www.k-net.bosai.go.jp) as shown in Fig. 2. This observation station is near to the coastal line of pacific ocean, therefore, the chosen input earthquake wave in the analysis is similar as close as possible with the real seismic wave propagating to the breakwater foundation.

It is noted that the earthquake composed of a major shock and two aftershocks lasts for 42.25 munities. The first shock (major shock) lasted for 5 min with a maximum acceleration of 85 gal and the second shock (first aftershock) also lasted for 5 min with a maximum acceleration of 25 gal while the third shock (second aftershock) lasted for 2.25 min with a maximum acceleration of 3 gal as shown in Fig.3. The interval between the first shock and the second shock was approximate 24 min, and the interval between the second shock and the third shock was approximate 6 min. It should be mentioned herein that such a long duration of motions has been the major cause of the severe liquefaction and ground deformation.

Newmark-method is used and the integration time interval is 0.01s. Rayleigh type of initial-rigidity-proportional attenuation is used and the damping values of the soils, the structure and the piles are assumed to be 2% and 10% for the first and second modes respectively in the dynamic analysis of the breakwater and foundation system.

Calculation steps

The analysis was performed in three steps:
Step 1: The static analysis considering the ground foundation-breakwater as a whole system is carried out to get the initial effective stress of the ground before the dynamic analysis. The distribution of initial mean effective stress caused by the gravity of ground and breakwater is shown in Fig. 4.

Step 2: Effective stress based soil water fully coupled dynamic analysis to investigate the seismic behavior of ground and breakwater during earthquake loading. In this step, static consolidation process followed by each earthquake shock is considered. Excess pore water pressure would develop in liquefiable sand layer, and the ground deformation would begin to accumulate.

Step 3: The long-term static analysis after earthquake loading, considering a complete consolidation in 3.5 years to examine the post-seismic behavior of breakwater and ground soil. The detailed loading process is listed in Table 5.

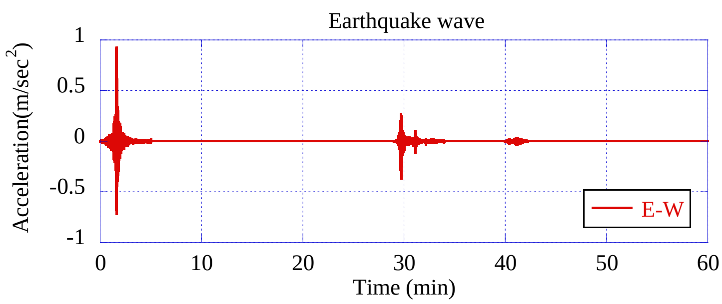

Figure 2. Recorded earthquake loading in E-W direction during the 2011 Great East Japan Earthquake

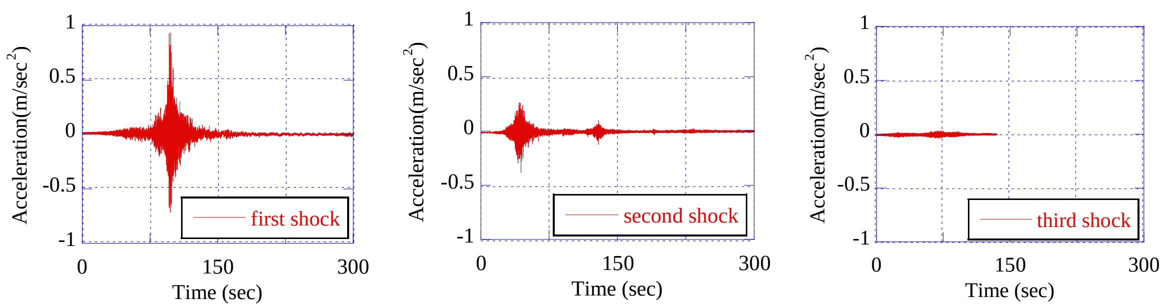

Figure 3. Three shocks of the earthquake loading during the 2011 Great East Japan Earthquake

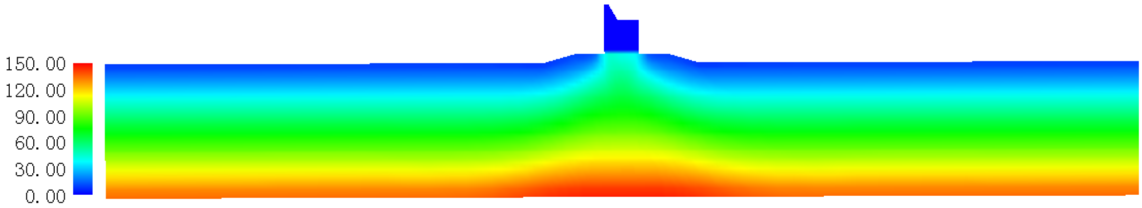

Figure. 4 Distribution of initial mean effective stress in the breakwater and foundation system due to gravity (unit: kPa)

Results and discussions

Seismic responses of breakwater and foundation soil

The seismic responses of breakwater and foundation soil under the earthquake loading are investigated. Fig.5 shows the horizontal acceleration responses of P-1 at the top of breakwater and P-2 at the bottom of caisson under the earthquake loading. The acceleration seismic responses at the two points are very similar and the amplification from the bottom of caisson to the top of breakwater is not obvious. However, the acceleration seismic responses are damped out by soil in the middle sand layer comparing with the input earthquake wave as shown in Fig. 6. The peak value of horizontal acceleration decreases obviously for the soil in liquefiable sand layer (GL-15 m), while the seismic wave was transmitted well in the upper clay layer (GL-5 m & GL-0 m). The amplitude of acceleration decreased as the building up of excess pore water pressure (Su et al. 2013) [39], and the soil's shear strength is reduced, which hampers effective propagation of shear waves to the soil surface. As the EPWPR value was larger at the middle sand layer (Fig. 8), the accelerations were highly attenuated relative to the base input (Fig. 6). Moreover, the attenuation of acceleration due to the loss of soil stiffness and strength was more significant in the near filed than that in the far field at the up clay layer. It was confirmed by Fig. 7 of the relationship between shear strain and shear stress, that larger shear strain in near field than that in far field was considered to be influenced by the replaced sand soil with high permeability below the breakwater structure.

Table 5. Loading process in liquefaction-consolidation analysis (a major shock followed by two aftershocks)

Step	Analysis type	Loading type	Calculation time (min)
1	Dynamic analysis	Major shock	5.00 (300 sec)
2	Static analysis	Consolidation	24.00 (1440 sec)
3	Dynamic analysis	First aftershock	5.00 (300 sec)
4	Static analysis	Consolidation	6.00 (360 sec)
5	Dynamic analysis	Second aftershock	2.25 (135 sec)
6	Static analysis	Consolidation	3.5 years

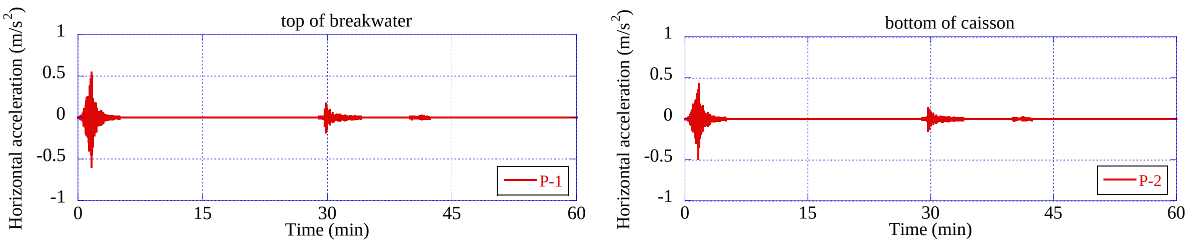

Figure 5. Horizontal acceleration responses of breakwater under earthquake loading

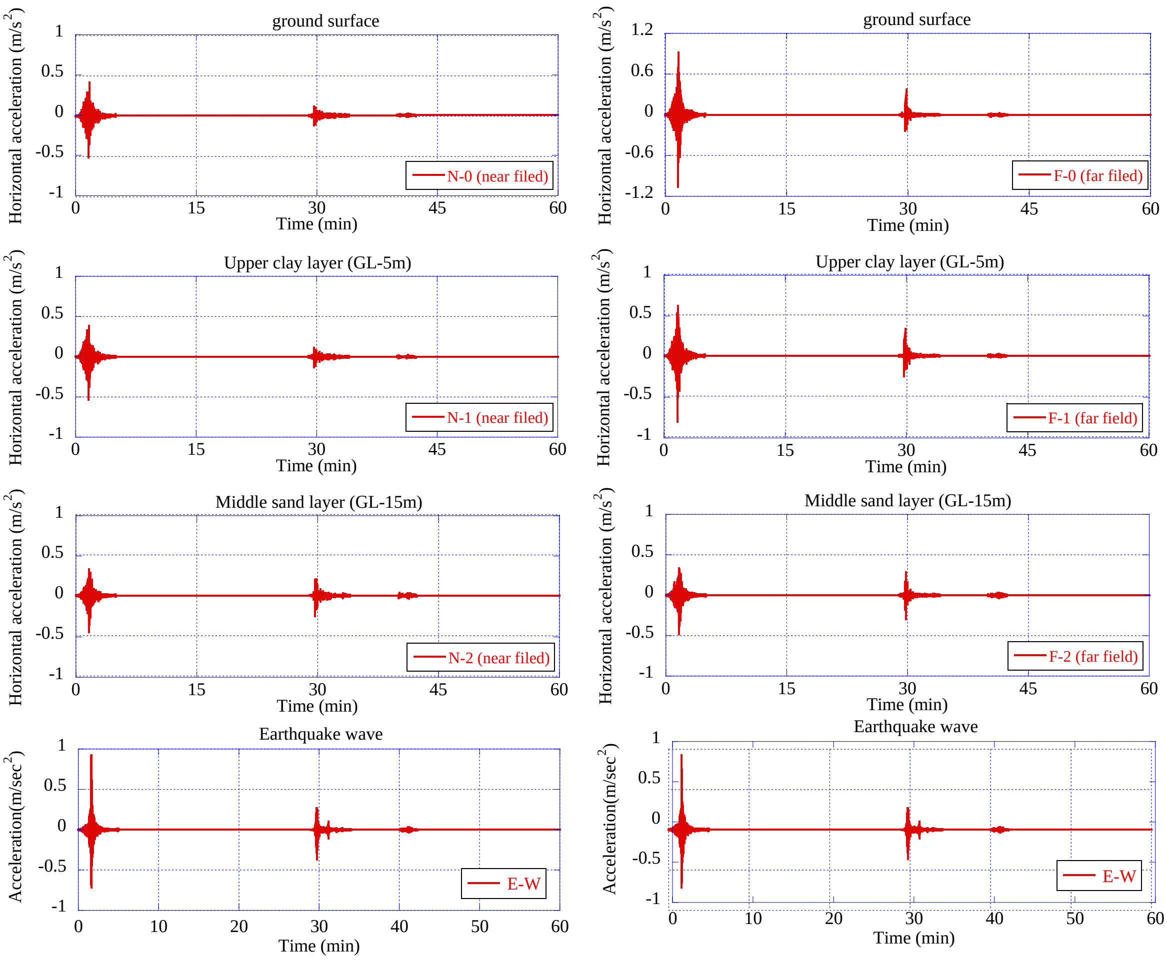

(a) Near field (b) Far field

Figure 6. Horizontal acceleration responses at different depth of foundation soil under earthquake loading

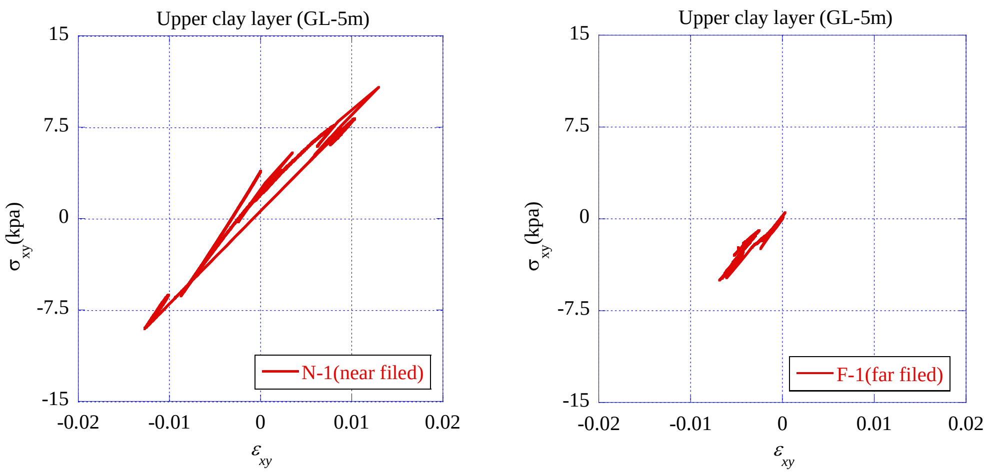

(a) Near field (b) Far field

Figure 7. Comparison of shear stress-strain relationship in upper clay layer in near field and far field

Liquefaction analysis

Fig. 8 shows the time history of excess pore water pressure ratio (EPWPR), which is defined as the ratio of excess pore water pressure (EPWP) to the initial vertical effective stress, at the selected location (see Fig. 2 for locations of these points). Comparing the results in upper clay with that in middle sand layer, it was clear that liquefaction occurred seriously in middle sand layer. The EPWPR values were significantly smaller at upper clay layer and replaced sand region (GL-5 m) throughout the shaking, revealing the clay soil and replaced sand had not yet liquefied. A small aftershock (the second shock) caused rapid increase in EPWPR, re-liquefying the middle sand layer (GL-15 m) at both near and far field and beneath the breakwater. EPWPR continued to increase and remained significantly larger until the end of earthquake. The dissipation of EPWP was in a slower rapid in near and far field than that in the region beneath breakwater, which could cause a slower rate of the settlement accumulation in near and far field than that beneath the breakwater. Obviously, this was attributed to the high permeability of the replaced sand soil beneath the breakwater structure.

As shown in Fig. 9, excess pore water generated rapidly with the highest value in middle sand layer below breakwater, in near field and far field. It is clear that liquefaction occurs at the end of the first shock, however, the liquefaction area become large at the end of the second shock, and at the end of the third shock, large area of liquefaction still remains in the middle sand layer. The thicker the upper clay layer is, the longer the duration of liquefaction is. This is because the dissipation of large excess pore pressures generated in the deeper depth leads to a longer duration of flow to the shallower depth. In addition, the replaced sand soil beneath breakwater is not fully liquefied during the whole earthquake loading because of its high permeability and the overlying breakwater structure which constricted soil liquefaction. Moreover, the replaced sand soil beneath breakwater might have reduced the degree of liquefaction of the soil lying below around the centerline and allowed the lateral stretching of the soil below the replaced sand towards the free field.

Fig. 10 shows the dissipation process of EPWP. The pore water was accumulated in middle sand layer beneath the clay layer as the clay layer acted as the barrier for vertical dissipation of EPWP. It was found that EPWP remains for a longer period of time in middle sand layer below upper clay layer compared with the region below the replaced sand soil. In the region around centerline below breakwater, EPWP become much lesser and the dissipation was quite faster after earthquake shakings (after t = 4 hours shown in Fig. 10). This might be due to the reason that the presence of replaced sand region underneath breakwater distributes the out flow of pore water. Overall, the dissipation of pore water was concentrated through the discontinuity region below the breakwater and finally towards the ground surface, contracting the foundation soil below breakwater and inducing additional settlement after shaking. In another word, EPWP remained for a longer period of time at discontinuous regions in non-homogeneous soil deposits, manifesting a larger settlement at that corresponding region causing non-uniform settlements. A significant amount of non-uniform settlement took place during and after earthquake shaking as shown in Figs.11&12. The value of EPWP build-up beneath breakwater was larger than that in other locations, which caused larger amount of settlement at breakwater than at ground surface in near and far field. The total amount of settlements at ground surface in near field and far field are 0.697 m and 0.688 m respectively, which was smaller than the settlement of the breakwater with a value of 0.815 m after complete consolidation of the ground as shown in Table 6. Obviously, the aftershock (the second shock) caused additional amount of settlement to breakwater structure (Fig. 11). The settlements occurred during earthquake shakings are almost the same at ground surface in both near field and far filed except for the small amount of heave at ground surface in the near filed (Fig. 12). However, the settlement developed faster in near filed than that in far field under post-earthquake consolidation process because of the quick out flow of pore water from near filed to the replaced sand region. As the pore water pressure dissipated mainly through the discontinuity, the complete dissipation took a long period of time, about 3.5 years (Fig.

10). An additional breakwater settlement of 0.277 m was measured due to post-seismic and dissipation of EPWP. The heaving at ground surface in near field occurring during the main shock shaking also settled down to a final settlement of 0.697m.

The total amount of settlements of ground in near field and far field were smaller than the settlement of the breakwater after complete consolidation of the ground. This might be due to the lager volume strain of replaced sand soil underneath breakwater during the dissipation of pore water. As the settlement induced due to dissipation of pore water after earthquake shaking were significantly larger in near field (0.549 m) and far field (0.547 m) than that at breakwater (0.277 m), dissipation of EPWP became the major factor after the earthquake shaking stopped, which caused larger amount of additional ground settlement than that during earthquake shaking.

Table 6. Amount of settlement at different positions (Unit: m)

Time	P-1	N-0	F-0
At the end of earthquake	0.538	0.148	0.141
3.5 years after earthquake	0.815	0.697	0.688

Deformation of the breakwater and foundation system

From Figs. 11&12 of the time histories of vertical displacements at top of breakwater and ground surface in both near field and far field, as mentioned above, a total settlement of 0.815 m for breakwater structure was observed, of which 0.538 m (66%) was measured during the main shock shaking (Table. 6). The main mechanisms that contribute to the settlement of foundation on a liquefied soil layer are volumetric compaction and shear deformation of the soil mass underneath the foundation. Shear deformation is accompanied by the lateral spreading of the non-liquefied soil below the structure which is initiated when the soil in the free field adjacent to the underlying soil on either side of the breakwater liquefies and loses its shear strength and allows the newly unconstrained soil below the breakwater collapse vertically and spread outwards. This type of settlement causes considerable vertical strain with no volume change. Concurrently, volumetric compaction of the sand mass under the upper clay layer occurs which results in both vertical and volumetric strains. This settlement results in the disruption of soil structure and rearrangement of soil grains and is the main mechanism responsible for the settlement in the free field (Maharjan & Takahashi 2014) [20]. It is difficult to separate the volumetric compaction effect from the shear deformation effect beneath the breakwater as they both happen at the same time. The final mechanism involved in the foundation soil settlement is the long-term dissipation of the excess pore pressure (consolidation).

From Table 6 of the calculated values for the settlement at the end of earthquake and final settlements of the breakwater and ground surface, as mentioned above, most part of the breakwater settlement (66%) accumulated during earthquake shaking. After ending of the earthquake shaking, the settlement of breakwater increases with a lower rate and ceases to increase when dissipation of excess pore pressure is completed. However, for the settlement of ground surface in both near field and far field, it is notable that the significant part of the settlement takes place in the process of pore pressure dissipation after the end of earthquake shaking (78.8% and 79.5% in the near field and far field, respectively). The calculated settlements of breakwater and ground surface differ to some extent from each other. This difference can be attributed to the upper clay layer that hindered the dissipation of pore water for near and far filed soil, and conversely, the replaced sand soil beneath the breakwater structure that accelerated the dissipation of pore water around centerline below the breakwater.

Obviously, the overall deformation of the ground around breakwater was large as shown in Fig.13 of displacement vector of breakwater and foundation system. The soil near breakwater translated sideways and lateral deformation was observed at the two sides of breakwater during earthquake shaking, especially in the middle sand layer that was found to laterally spread on both sides towards the free field. This caused serious settlement of breakwater. Shear deformation of underlying liquefied sand and volumetric change due to pore water dissipation are also factors for breakwater and ground settlements. As the presence of the upper clay layer acted as a hindrance and it took about 3.5 years for the water complete its dissipation through the discontinuous region according to the calculation results.

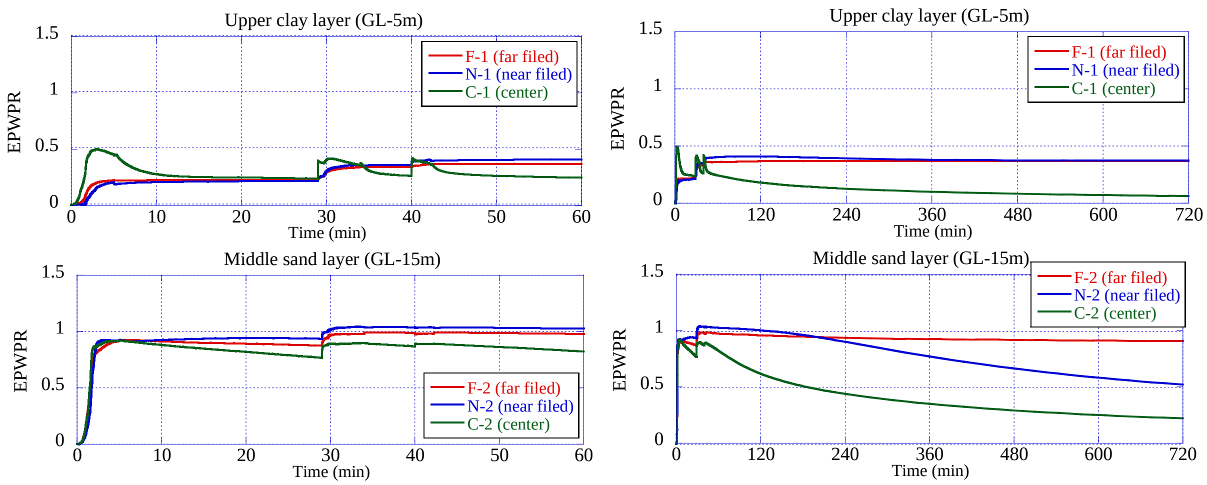

(a) Within 60 minutes (b) Within720 minutes

Figure 8. Time history of EPWPR at different depth of foundation soil

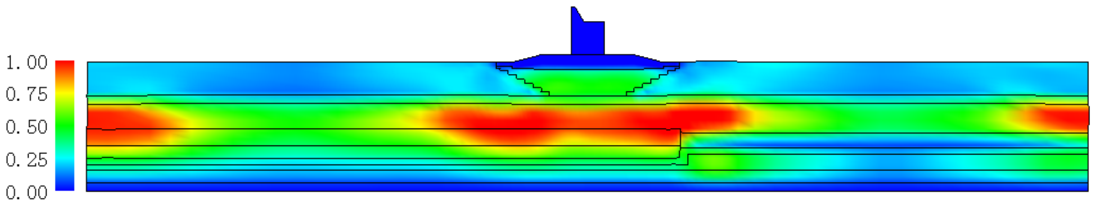

(a) At the end of the first shock (t = 5 minutes)

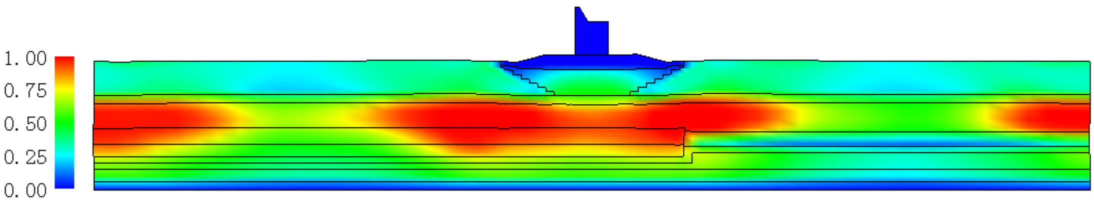

(b) At the end of the second shock (t = 34 minutes)

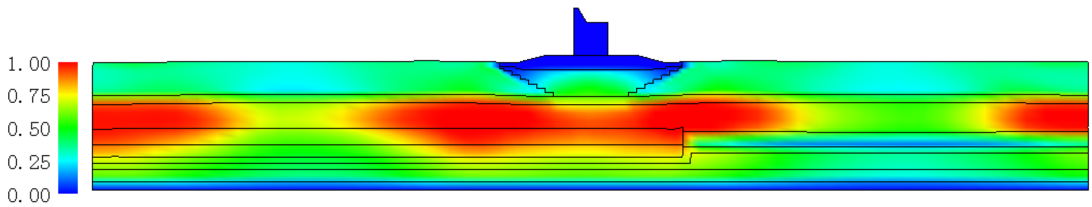

(c) At the end of the third shock (t = 42.25 minutes)

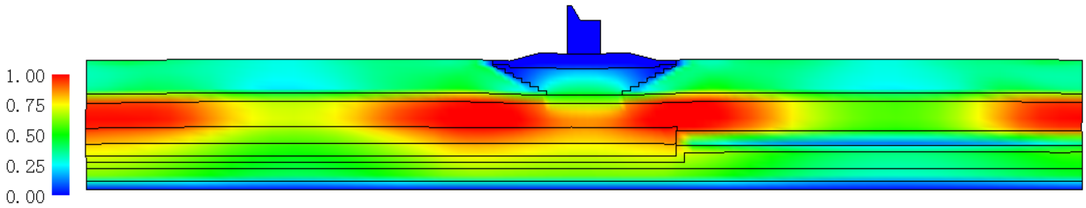

(d) After earthquake shaking (t = 1 hour)

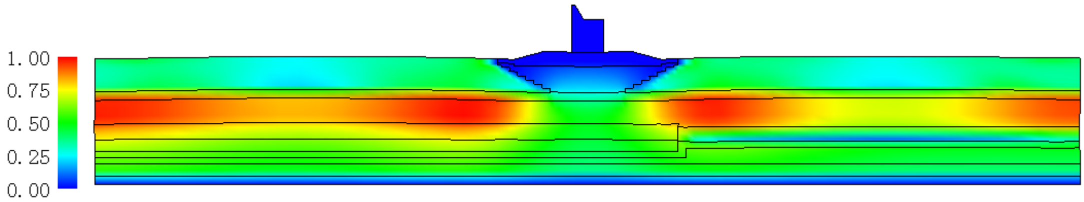

(e) After earthquake shaking (t = 4 hours)

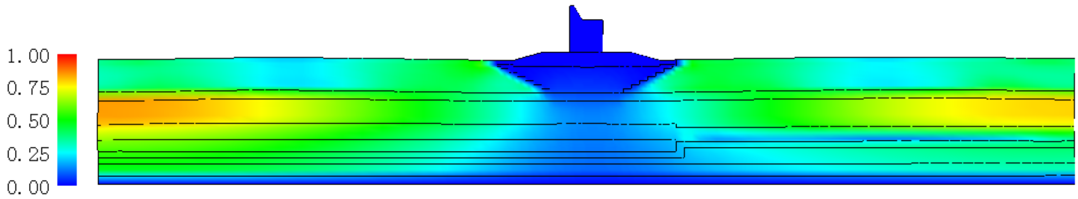

(f) After earthquake shaking (t = 1.3 days)

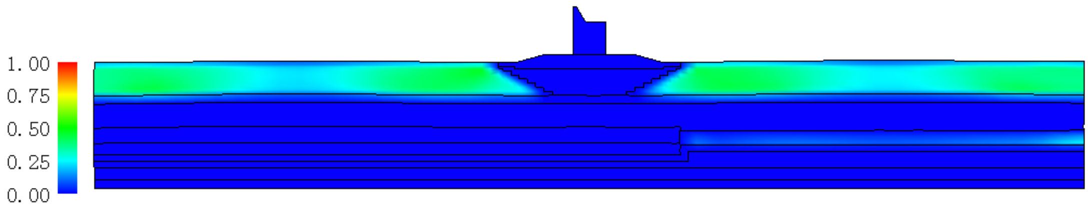

(g) After earthquake shaking (t = 13 days)

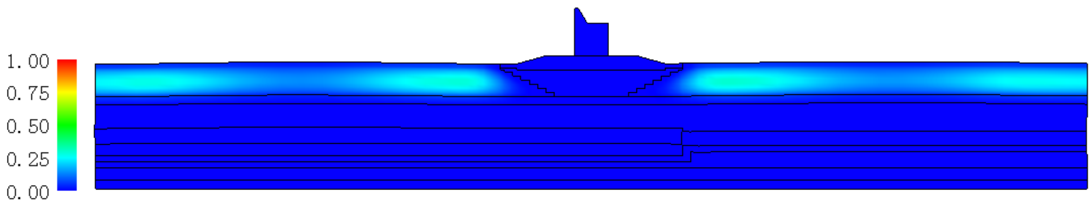

(h) After earthquake shaking (t = 130 days)

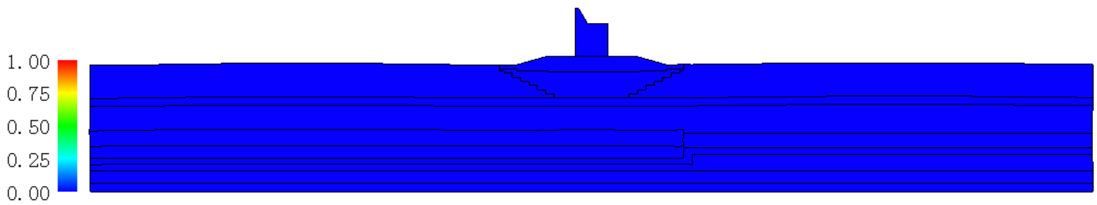

(i) After earthquake shaking (t = 3.5 years, complete dissipation of EPWP)

Figure 9. Distribution of Excess pore water pressure ratio at different time

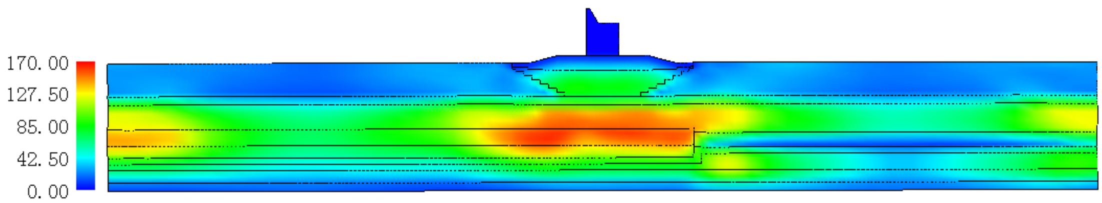

(a) At the end of the first shock (t = 5 minutes)

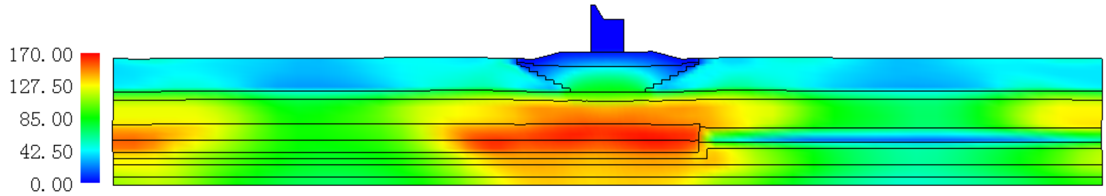

(b) At the end of the second shock (t = 34 minutes)

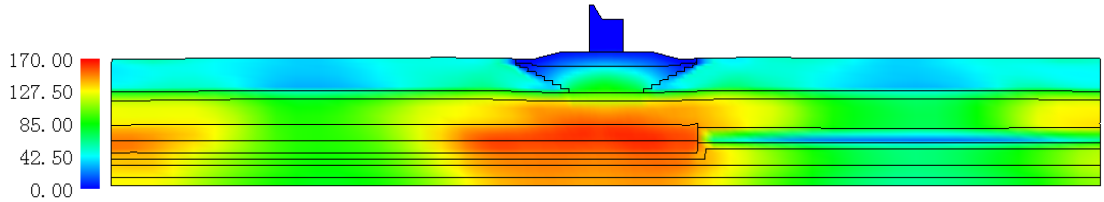

(c) At the end of the third shock (t = 42.25 minutes)

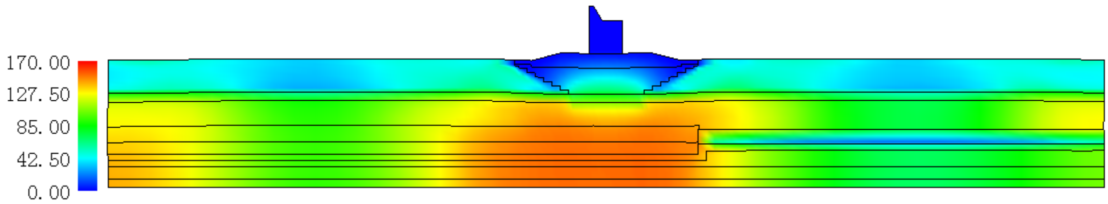

(d) After earthquake shaking (t = 1 hour)

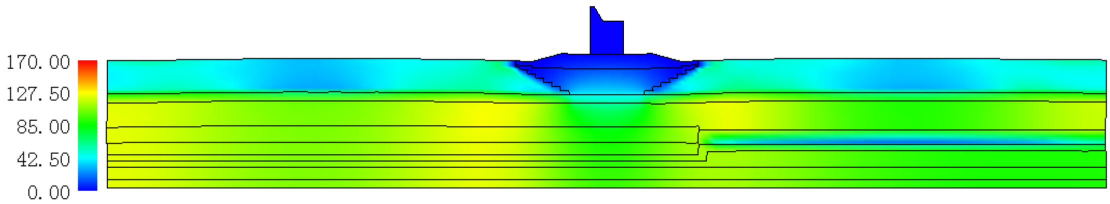

(e) After earthquake shaking (t = 4 hours)

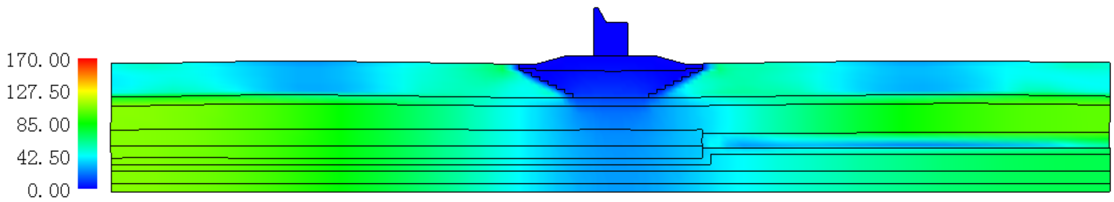

(f) After earthquake shaking (t = 1.3 days)

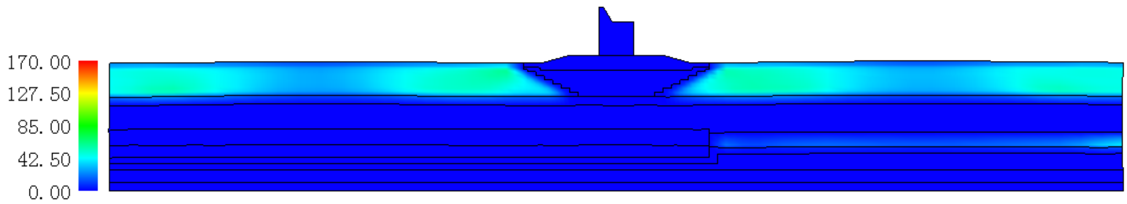

(g) After earthquake shaking (t = 13 days)

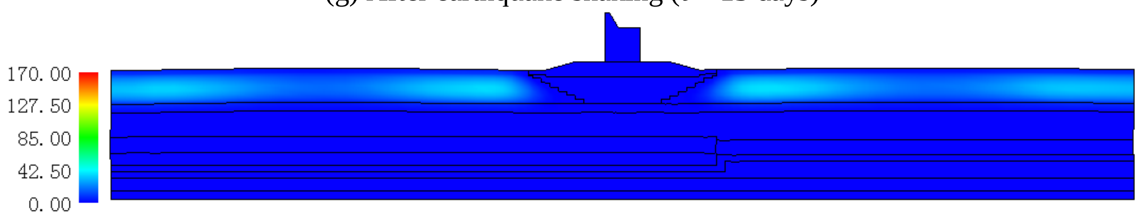

(h) After earthquake shaking (t = 130 days)

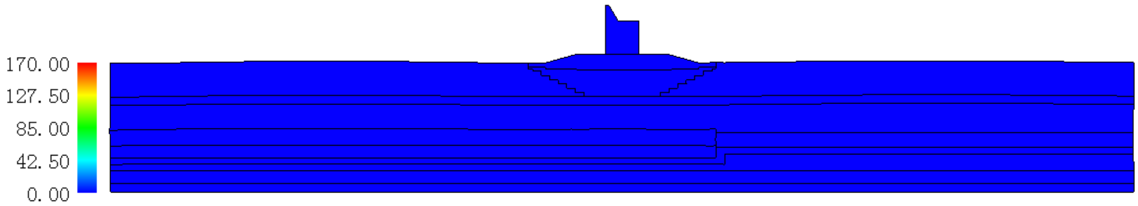

(i) After earthquake shaking (t = 3.5 years, complete dissipation of EPWP)

Figure 10. Dissipation process of excess pore water pressure (unit: kPa)

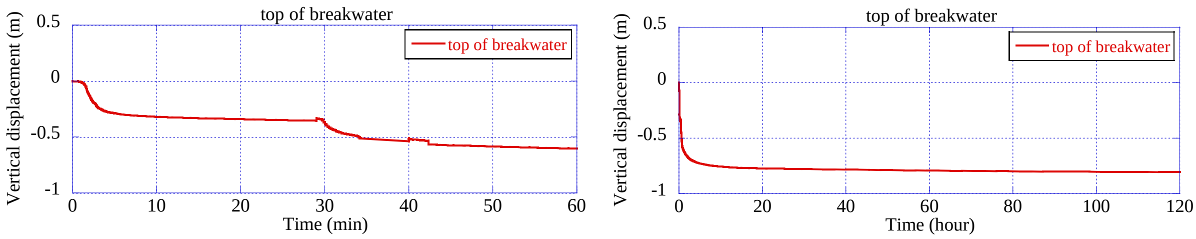

(a) Within 60 minutes (b) Within120 hours

Figure 11. Time history of vertical displacement at the top of breakwater

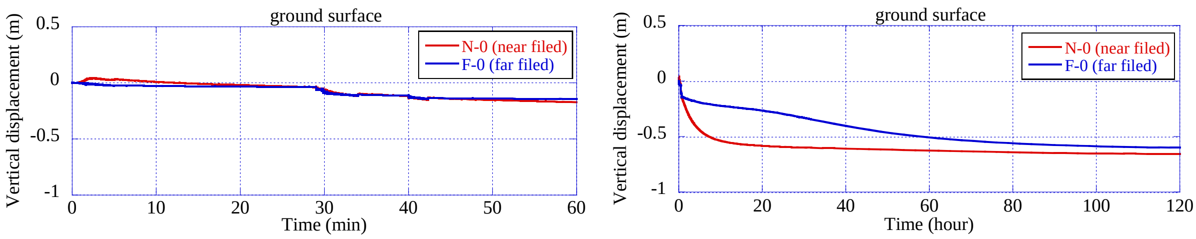

(a) Within 60 minutes (b) Within120 hours

Figure 12. Time history of vertical displacement at ground surface in near field and far field

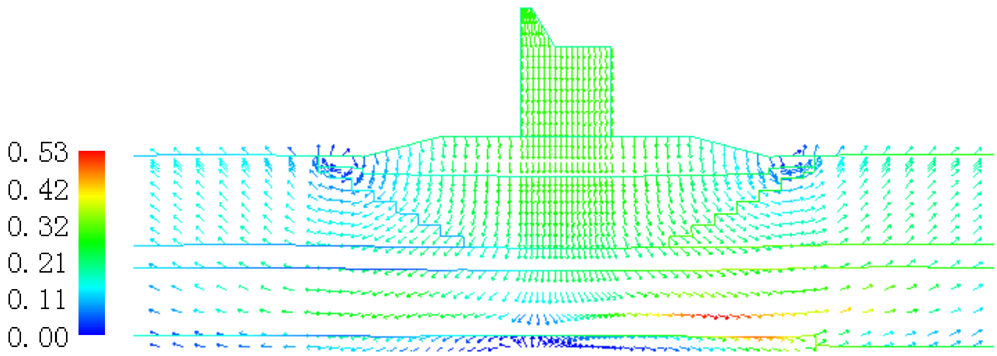

(a) At the end of the first shock (unit: m)

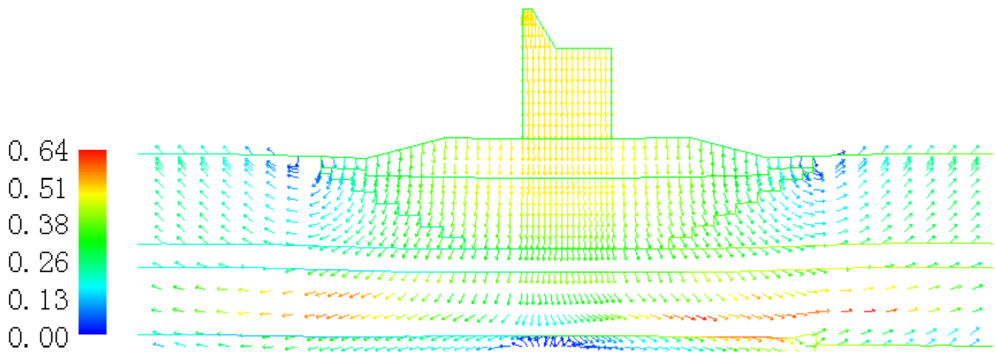

(b) At the end of the second shock (unit: m)

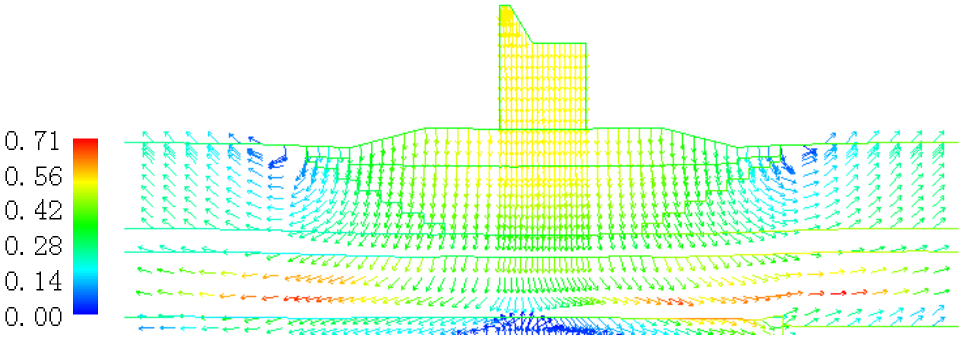

(c) At the end of the third shock (unit: m)

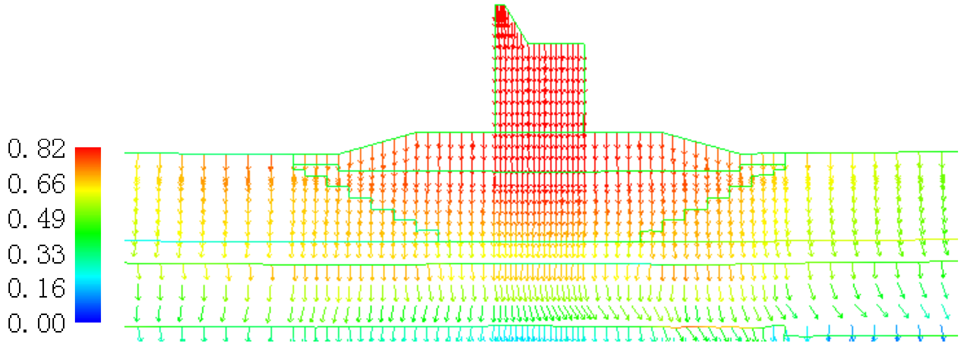

(d) After complete dissipation of EPWP (unit: m)

Figure 13. Displacement vector of breakwater and foundation system during and after earthquake loading (A part of mesh)

Conclusions

In this study, the co-seismic and post-seismic performance of a caisson type breakwater resting on the natural ground with discontinuous low permeability an liquefiable layers subjected to the 2011 Great East Japan Earthquake is investigated using soil-water coupled finite element method. Based on the calculated results, the following conclusions can be drawn:

1. The repeated earthquake shaking has a significant effect on the accumulated deformation of embankments. The second aftershock caused an increase in EPWP generation and an additional settlement. Moreover, the effects of aftershocks were more pronounced in the non-homogeneous liquefiable foundations, leading to the post-liquefaction delayed settlement and this conclusion was also confirmed by Maharjan and Takahashi (2014) [20].
2. The replaced sand region with a high permeability has faster dissipation of pore water while the dissipation continued for a longer time period in near and far field of ground, accumulating delayed displacements. Overall, the dissipation of pore water was concentrated through the discontinuity region below the breakwater and finally towards the ground surface, contracting the foundation soil and inducing additional settlement after shaking and causing larger amount of settlement on breakwater than that on ground surface in near and far filed.
3. The accumulation of pore water beneath the low permeability upper clay layer induced large shear strain in middle sand layer, resulting large amount of lateral spreading. Lateral spread, shear deformation of underlying liquefied sand and volumetric change due to pore water dissipation are the main factors for breakwater and ground

settlements. The presence of the upper clay layer acted as a hindrance and it took about 3.5 years for the water complete its dissipation through the discontinuous region according to the calculation results.

4. The thick clay layer may cause long term consolidation process while the thick sand layer may bring a large area of liquefaction and severe ground deformation. Although the replaced sand soil beneath breakwater structure can improve ground bearing capacity, it may cause the risk of large amount of settlement to breakwater, which can reduce capacity of the breakwater to resist tsunami after earthquake loading.

Acknowledgements

This work was supported by National Nature Science Foundation of China (Grant No. 51308346), Guangdong Natural Science Foundation (Grant No. 2014A030313551), Natural Science Foundation of SZU (Grant No.201420), Foundation of Key Laboratory of Geotechnical and Underground Engineering (KLE-TJGE-B1504) and Scientific and Technical Innovation Foundation of Shenzheng (Grant No. JCYJ20150324140036839).

References

[1] Seed, H.B. (1968) Landslides during earthquakes due to liquefaction, *J Mech Found Div* 1968; **94**(5), 1055–123.
[2] Adalier, K., Elgamal, A.W., Martin, G.R. (1998) Foundation liquefaction countermeasures for earthembankments, *J Geotech Geoenviron Eng* **124** (6), 500–17.
[3] Huang, Y., Yu, M. (2013) Review of soil liquefaction characteristics during major earthquakes of the twenty-first century, *Natural Hazards* **65**, 2375-2384.
[4] Oka, F., Tsai, P., Kimoto, S., Kato, R. (2012) Damage patterns of river embankments due to the 2011off the Pacific Coast of Tohoku earthquake and a numerical modeling of the deformation of river embankments with a clayey subsoil layer, *Soils Found* **52**(5), 890–909.
[5] Mori, N., Cox, D.T., Yasuda, T., Mase, H. (2013) Overview of the 2011 Tohoku Earthquake Tsunami damage and relation with coastal protection along the Sanriku coast, *Earthquake Spectra* **29**(S1), S127–S143.
[6] Mori, N., Yoneyama, N., Pringle, W. (2015) Effects of the Offshore Barrier Against the 2011 Off the Pacific Coast of Tohoku Earthquake Tsunami and Lessons Learned, Post-Tsunami Hazard, *Advances in Natural and Technological Hazards Research* **44**, 121-132.
[7] Fujima, K. (2006) Effect of a submerged bay-mouth breakwater on tsunami behavior analyzed by 2D/3D hybrid model simulation, *Natural Hazards* **39** (2), 179-193.
[8] Imase, T., Maeda, K., Miyake, M., Sawada, Y., Sumida. H., Tsurugasaki, K. (2012) Destabilization of a caisson-type breakwater by scouring and seepage failure of the seabed due to a tsunami, *Proceedings of International Conference on Scour and Erosion*, 128–135.
[9] Susumu, I. (2012) Combined Failure Mechanism of a Breakwater Subject to Tsunami during 2011 East Japan Earthquake, *Geological and Earthquake Engineering* **37**, 177-186.
[10] Takahashi, H., Sassa, S., Morikawa, Y., Takano, D., Maruyama, K. (2014) Stability of caisson-type breakwater foundation under tsunami-induced seepage, *Soils and Foundations* **54** (4), 789-805.
[11] Memos, C., Kiara, A., Pavlidis, E. (2003) Coupled seismic response analysis of rubble-mound breakwater, *Water and Maritime Engineering* ICE, 23–31
[12] Yuksel, Y., Cetin, K.O., Ozguven, O., Isik, N.S., Cevik, E., Sumer, B.M. (2004) Seismic response of a rubble mound breakwater in Turkey, *Proc Inst Civil Eng: Marit Eng* **157**(4), 151–161.
[13] Jafarian. Y., Alielahi. H., Abdollahi, A.S., Vakili, B. (2010) Seismic numerical simulation of breakwater on a liquefiable layer: Iran LNG port, *Electron J Geotech Eng* 15D, 1–11.
[14] Ye, J.H. (2012) Seismic response of poro-elastic seabed and composite breakwater under strong earthquake loading, *Bulletin of Earthquake Engineering* **10**(5), 1609-1633.
[15] Aydingun, O., Adalier. K. (2003) Numerical analysis of seismically induced liquefaction in earth embankment foundations. PartI. Bench mark model, *CanGeotech J* **40**(4), 753–65.
[16] Adalier, K., Sharp, M.K. (2004) Embankment dam on liquefiable foundation-dynamic behavior and densification remediation, *J Geotech Geoenviron Eng* **130** (11), 1214–24.
[17] Ye, J.H., Wang, G. (2015) Seismic dynamics of offshore breakwater on liquefiable seabed foundation, *Soil Dynamics and Earthquake Engineering* **76**, 86-99.
[18] Huang, Y., Bao, Y.J., Zhang, M., Liu, C., Lu, P. (2015) Analysis of the mechanism of seabed liquefaction induced by waves and related seabed protection, *Natural Hazards* **79**, 1399-1408.
[19] Zhang, S., Wang, G., Sa, W. (2013) Damage evaluation of concrete gravity dams under mainshock–aftershock seismic sequences, *Soil DynEarthqEng* **50**, 16–27.

[20] Maharjan, M., Takahashi, A. (2014) Liquefaction-induced deformation of earth embankments on non-homogeneous soil deposits under sequential ground motions, *Soil Dynamics and Earthquake Engineering* **66**,161–9.
[21] Ye, B., Ye, G.L., Zhang, F., Yashima, A. (2007) Experiment and numerical simulation of repeated liquefaction-consolidation of sand, *Soils Found* **47**(3), 547–58.
[22] Xia, Z.F., Ye, G.L., Wang, J.H., Ye, B., Zhang, F. (2010) Fully coupled numerical analysis of repeated shake-consolidation process of earth embankment on liquefiable foundation, *Soil Dyn Earthq Eng* **30**(11), 1309–18.
[23] Sasaki, Y., Towhata, I., Miyamoto, K., Shirato, M., Narita, A., Sasaki, T., Sako, S. (2012) Reconnaissance report on damage in and around river levees caused by the 2011off the Pacific coast of Tohoku earthquake, *Soils Found* **52** (5), 1016–32.
[24] Ye, G.L. (2011) DBLEAVES: User's manual Version 1.6. *Shanghai Jiaotong University* (In Japanese and Chinese) China.
[25] Zhang, F., Ye, B., Noda, T., Nakano, M., Nakai, K. (2007) Explanation of cyclic mobility of soils: approach by stress-induced anisotropy, *Soils and Foundations* **47**(4), 635-648.
[26] Zhang, F., Ye, B., Ye, G.L. (2011) Unified description of sand behavior, *Frontiers of Architecture and Civil Engineering in China* **5**(2), 121–150.
[27] Iai, S., Ichii, K., Liu, H.L. (1998) Effective stress analysis of port structures, *Soils Found* (Special Issue of Geotechnical Aspects of the January 17, 1995 Hyogoken Nambu Earthquake) (2), 97–114.
[28] Hashiguchi, K., Ueno, M. (1977) Elastoplastic constitutive laws of granular material, Constitutive Equations of Soils, *Proc. 9th Int. Conf. Soil Mech. Found. Engrg., Spec*. Ses. 9, Murayama, S. and Schofield, A. N. (eds.) Tokyo, JSSMFE: 73-82.
[29] Asaoka, A., Noda, T., Yamada, E., Kaneda, K., Nakano, M. (2002) An elasto-plastic description of two distinct volume change mechanisms of soils, *Soils and Foundations* **42**(5), 47-57.
[30] Ye, B., Ye, G.L., Zhang, F. (2012) Numerical modeling of changes in anisotropy during liquefaction using a generalized constitutive model, *Computers and Geotechnics* **42**, 62-72.
[31] Ye, G.L., Sheng, J.R., Ye, B., Wang, J.H. (2012) Automated true triaxial apparatus and its application to over-consolidated clay, *Geotechnical Testing Journal* **35**(4), 517-528.
[32] Ye, G.L., Ye, B., Zhang, F. (2013) Strength and dilatancy of overconsolidated clays in drained true triaxial tests, *Journal of Geotechnical and Geo-environmental Engineering*, **140**(4), 06013006.
[33] Ye, B., Ye, G.L., Zhang, F., Yashima, A. (2007) Experiment and numerical simulation of repeated liquefaction-consolidation of sand, *Soils and Foundations*, **47** (3), 547-558.
[34] Zhang, F., Jin, Y., Ye, B. (2010) A try to give a unified description of Toyoura sand, *Soils and Foundations* **50** (3), 679-693.
[35] Jin, Y., Bao, X.H., Kondo, Y., Zhang, F. (2010) Soil-water coupling analysis of real-scale field test for 9-pile foundation subjected to cyclic horizontal loading. *Geotechnical Special Publication, Deep Foundation and Geotechnical in situ Test ASCE* **205**,111-118.
[36] Bao, X.H., Morikawa, Y., Kondo, Y., Nakamura, K., Zhang, F. (2012) Shaking table test on reinforcement effect of partial ground improvement for group-pile foundation and its numerical simulation, *Soils and Foundations* **52**(6), 1043-1061.
[37] Bao, XH., Ye, B., Ye, G.L., Sagou, Y. and Zhang, F. (2014) Seismic performance of SSPQ retaining wall-centrifuge model tests and numerical evaluation, *Soil Dynamics and Earthquake Engineering* **61-62**, 63-82.
[38] Bao, X.H., Ye, G.L., Ye, B. and Zhang, F. (2016) Co-seismic and post-seismic behavior of an existed shallow foundation and super structure system on a natural sand/silt layered ground, *Engineering Computations* **33**(1), 288-304.
[39] Su, D., Ming, H.Y., Li, X.S. (2013) Effect of shaking strength on the seismic response of liquefiable level ground, *Engineering Geology* **166**, 262-271.